Design of an Efficient Pumping Scheme for Mid-IR Dy^{3+}:$Ga_5Ge_{20}Sb_{10}S_{65}$ PCF Fiber Laser

Mario Christian Falconi, *Student Member, IEEE*, Giuseppe Palma, Florent Starecki, Virginie Nazabal, Johann Troles, Stefano Taccheo, Maurizio Ferrari, and Francesco Prudenzano

***Abstract*— This letter illustrates the design of a novel medium infrared (Mid-IR) laser based on a photonic crystal fiber made of dysprosium-doped chalcogenide glass, Dy^{3+}:$Ga_5Ge_{20}Sb_{10}S_{65}$. In order to perform a realistic investigation, the simulation is performed by taking into account the spectroscopic parameters measured on the rare earth-doped glass sample. The simulated results show that an optical beam emission close to 4400-nm wavelength can be obtained by employing two pump beams at 2850 nm (pump #1) and 4092 nm (pump #2) wavelengths. The pump beams can be provided by commercial quantum cascade lasers. As example, for the pump powers of 50 mW (pump #1) and 1 W (pump #2), the input mirror reflectivity of 99%, the output mirror reflectivity of 30%, and the optical cavity length of 50 cm, a signal power close to 350 mW at the wavelength of 4384 nm can be generated. This result indicates that the designed source configuration is feasible for high beam quality Mid-IR light generation and it is efficient enough to find applications in optical free propagation links, optical remote sensing, and medicine.**

***Index Terms*— Chalcogenide glass, medium infrared, dysprosium, laser.**

I. Introduction

LIGHT SOURCES operating in the medium infrared (Mid-IR) wavelength range attract strong interest for their potential applications, ranging from lasing to active sensing in the field of medicine and environmental monitoring [1]–[8]. Chalcogenide glasses constitute optimal material hosts, which can be doped with suitable rare earths for the construction of Mid-IR lasers and amplifiers [9]–[14]. Dysprosium is one of the rare earths which can be exploited for the laser generation close to 4400 nm wavelength. Unfortunately, it exhibits a poor overall efficiency due to the long lifetime of its lower laser level $^6H_{13/2}$ [4]. Cascade lasing approach, employing an auxiliary idler signal, requires high fabrication complexity, related to the construction of two pairs of Bragg gratings and two lasing cavities [3], [4], [12]. Moreover, to the best of our knowledge, neither experimental evidence nor simulated results of high efficiency dysprosium doped fiber laser are reported in literature. Therefore, the investigation of more efficient pumping schemes is welcome with the aim of fabricating fiber lasers at these wavelengths.

In this letter, a novel and simple pumping configuration is proposed for the first time. The feasibility investigation is conducted numerically. A simulated pump efficiency of about 35 % is calculated. It is very high with respect to the literature results. We underline that the computer code confirms the poor laser efficiency achievable for the different pumping schemes, as reported in literature. The proposed PCF laser cavity can provide very high beam quality, typical of the single mode PCF guided light, in Mid-IR wavelength range, by employing commercial QCL pump lasers with minor quality beam characteristics at slightly shorter wavelengths. During the last years, high performance QCLs operating in the Mid-IR have been fabricated. Ultra-large wavelength tunability is one of their main strength points. Fiber lasers will not substitute, but will complement MQW lasers, as already happened in the visible and near-infrared wavelength intervals. The interest in this kind of source is motivated by the need of diffraction-limited Mid-IR laser beams, necessary in a number of technological challenges as optical free propagation links, optical remote sensing, laser therapy and diagnostics. Moreover, in addition to the excellent beam quality, fiber lasers provide high-power, broad continuum generation, and ultra-short pulse generation.

II. Theory and Design

The designed optical source employs a simple but optimized pumping scheme. Two optical pumps, with suitable wavelengths and powers, are injected within a single-mode photonic crystal fiber (PCF) by employing an optical combiner. An end pump combiner has two multi-mode pump input fiber legs and a single output fiber which is spliced to the Dy^{3+}:$Ga_5Ge_{20}Sb_{10}S_{65}$ fiber. The Dy^{3+}:$Ga_5Ge_{20}Sb_{10}S_{65}$ PCF laser is designed to obtain signal generation close to $\lambda_s = 4400$ nm wavelength. The optical cavity is obtained

Manuscript received February 6, 2016; revised May 16, 2016; accepted June 9, 2016. Date of publication June 15, 2016; date of current version July 13, 2016. This work was supported in part by the Ministero dell'Istruzione, dell'Università e della Ricerca under Grant PON01 01224, Grant PONa3 00298, and Grant PON02 00576 3329762, and in part by EU COST Action under Grant MP1401.

M. C. Falconi, G. Palma, and F. Prudenzano are with the Department of Electrical and Information Engineering, Politecnico di Bari, Bari 70125, Italy (e-mail: mariochristian.falconi@poliba.it; giuseppe.palma@poliba.it; francesco.prudenzano@poliba.it).

F. Starecki, V. Nazabal, and J. Troles are with the Centre National de la Recherche Scientifique, Institut des Sciences Chimiques de Rennes, Universit de Rennes, Rennes 35042, France (e-mail: virginie.nazabal@univ-rennes1.fr; johann.troles@univrennes1.fr; florent.starecki@univ-rennes1.fr).

S. Taccheo is with the Institute of Advanced Telecommunications, Swansea University, Swansea SA2 8PP, U.K. (e-mail: s.taccheo@swansea.ac.uk).

M. Ferrari is with the Characterization and Development of Materials for Photonics and Optoelectronics Laboratory, Consiglio Nazionale delle Ricerche-Istituto di Fotonica e Nanotecnologie, Trento 38123, Italy (e-mail: mferrari@science.unitn.it).

Color versions of one or more of the figures in this letter are available online at http://ieeexplore.ieee.org.

Digital Object Identifier 10.1109/LPT.2016.2581022

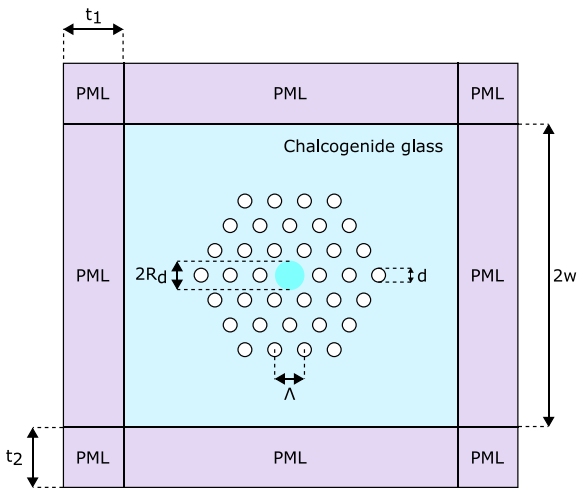

Fig. 1. Cross-section of the photonic crystal fiber.

by using two suitable fiber Bragg gratings (FBG1, FBG2) inscribed in the core. The PCF cross-section is depicted in Fig. 1. It allows single mode propagation at both the pump and signal wavelengths. Three rings of air holes surround the rare earth-doped solid core. The geometrical parameters are the following: hole-to-hole spacing (or pitch) $\Lambda = 8\,\mu$m, hole diameter $d = 3.2\,\mu$m, doped region radius $R_d = 4\,\mu$m. The design is performed by considering the measured PCF parameters reported in [9] and [11]. However, both the pumps could also be launched in a single core or in a double clad fiber. The measured refractive index wavelength dispersion of the $Ga_5Ge_{20}Sb_{10}S_{65}$ chalcogenide glass [9], [11] is taken into account by a Cauchy equation:

$$n(\lambda) = B + \frac{C}{\lambda^2} + \frac{D}{\lambda^4} \tag{1}$$

where $B = 2.2181$, $C = 0.0551$ and $D = -0.0003$. A full vectorial Finite Element Method (FEM) commercial code is employed for the PCF electromagnetic investigation. Perfectly matched layers (PMLs) are used to avoid the numerical drawbacks due to the reflections into the computational domain of the outgoing waves. The computational domain is a square having width $w = 48\,\mu$m. The PML thickness is $t_{PML} = 12\,\mu$m. Fig. 2 illustrates the electric field norm distribution of the fundamental mode at the wavelength $\lambda_s = 4384\,$nm.

The rare earth-light interaction is modelled as a three level laser system. The model employed in the simulation includes the pump absorption and stimulated emission close to the pump wavelengths $\lambda_{p1} = 2850\,$nm (pump #1) and $\lambda_{p2} = 4092\,$nm (pump #2), and the signal absorption and stimulated emission to the wavelength $\lambda_s = 4384\,$nm. The emission cross-sections spectra at $3.0\,\mu$m and $4.3\,\mu$m were both estimated using the Futchbauer-Ladenburg relation from fluorescence measurements (Fig. 3). The $3.0\,\mu$m absorption cross-section has been calculated from the absorption spectrum, while the $4.3\,\mu$m excited state absorption cross-section has been calculated from the emission cross-section using the reciprocity properties, also called the McCumber formula. These values

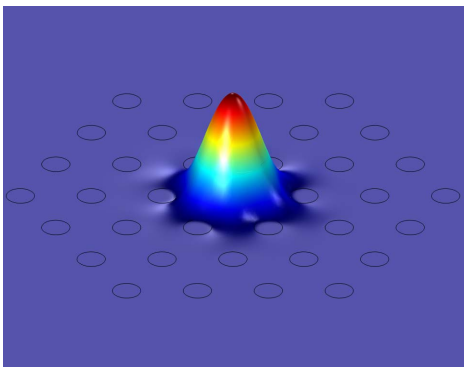

Fig. 2. Distribution of the electric field norm for the fundamental mode at signal wavelength $\lambda_s = 4384\,$nm.

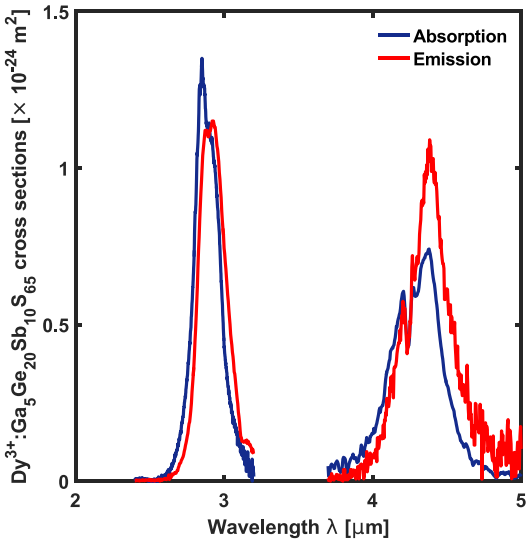

Fig. 3. Calculated emission and absorption cross-sections for the Dy^{3+}:$Ga_5Ge_{20}Sb_{10}S_{65}$ glass.

TABLE I
CALCULATED SPECTROSCOPIC PARAMETERS OF THE DY^{3+}-DOPED CHALCOGENIDE GLASS

Energy transition	Wavelength (nm)	Branching ratio	Lifetime (ms)
$^6H_{13/2} \rightarrow {}^6H_{15/2}$	2920	100 %	7.03
$^6H_{11/2} \rightarrow {}^6H_{13/2}$	4384	8.8 %	1.48
$^6H_{11/2} \rightarrow {}^6H_{15/2}$	1709	91.2 %	1.48

are in agreement with other calculated parameters in selenide matrix [2]–[4]. Table I reports the calculated branching ratios and fluorescence lifetimes taking into account calculated multiphonon relaxation [7]. Propagation losses $\alpha(\nu) = 3$ dBm^{-1} for all frequencies ν are supposed [4].

The rate equations (2) are:

$$\begin{bmatrix} C_{11} & C_{12} & C_{13} \\ C_{21} & C_{22} & C_{23} \\ C_{31} & C_{32} & C_{33} \end{bmatrix} \begin{bmatrix} N_1 \\ N_2 \\ N_3 \end{bmatrix} = \begin{bmatrix} 0 \\ 0 \\ N_{Dy} \end{bmatrix} \tag{2}$$

where $C_{11} = 0$, $C_{12} = W_{23}^p + W_{23}^s$, $C_{13} = -W_{32}^p - W_{32}^s - \frac{1}{\tau_3}$, $C_{21} = -W_{12}^p$, $C_{22} = W_{21}^p + \frac{1}{\tau_2}$, $C_{23} = \frac{\beta_{31}}{\tau_3}$ and

$C_{31} = C_{32} = C_{33} = 1$, $N_i(x, y, z)$ with $i = 1, 2, 3$ are the steady-state ion populations of the Dy^{3+} energy levels, $W_{ij} = \frac{\sigma_{ij}(\nu)}{h\nu} P(z)|E(x, y, \nu)|^2$ the transition rates, σ_{ij} the cross section pertaining the $i \rightarrow j$ transition, h the Planck constant, ν the optical frequency, $P(z)$ the optical mode power, $E(x, y, \nu)$ the normalized optical mode intensity, τ_i the lifetimes and β_{ij} the branching ratios.

The power propagation equations (3) are:

$$\begin{cases} \dfrac{\mathrm{d}P_{\mathrm{p1}}}{\mathrm{d}z} = g_{\mathrm{p1}}(z)P_{\mathrm{p1}}(z) - \alpha(\nu_{\mathrm{p1}})P_{\mathrm{p1}}(z) \\ \dfrac{\mathrm{d}P_{\mathrm{p2}}}{\mathrm{d}z} = g_{\mathrm{p2}}(z)P_{\mathrm{p2}}(z) - \alpha(\nu_{\mathrm{p2}})P_{\mathrm{p2}}(z) \\ \dfrac{\mathrm{d}P_{\mathrm{s}}^{+}}{\mathrm{d}z} = g_{\mathrm{s}}(z)P_{\mathrm{s}}^{+}(z) - \alpha(\nu_{\mathrm{s}})P_{\mathrm{s}}^{+}(z) \\ \dfrac{\mathrm{d}P_{\mathrm{s}}^{-}}{\mathrm{d}z} = -g_{\mathrm{s}}(z)P_{\mathrm{s}}^{-}(z) + \alpha(\nu_{\mathrm{s}})P_{\mathrm{s}}^{-}(z) \end{cases} \tag{3}$$

where $g_{\mathrm{p1}}(z) = -\sigma_{12}(\nu_{\mathrm{p1}})n_1(z, \nu_{\mathrm{p1}}) + \sigma_{21}(\nu_{\mathrm{p1}})n_2(z, \nu_{\mathrm{p1}})$, $g_{\mathrm{p2}}(z) = -\sigma_{23}(\nu_{\mathrm{p2}})n_2(z, \nu_{\mathrm{p2}}) + \sigma_{32}(\nu_{\mathrm{p2}})n_3(z, \nu_{\mathrm{p2}})$ and $g_{\mathrm{s}}(z) = -\sigma_{23}(\nu_{\mathrm{s}})n_2(z, \nu_{\mathrm{s}}) + \sigma_{32}(\nu_{\mathrm{s}})n_3(z, \nu_{\mathrm{s}})$.

$P_{\mathrm{p1}}(z)$, $P_{\mathrm{p2}}(z)$, $P_{\mathrm{s}}^{\pm}(z)$ are the optical powers for pump #1, pump #2 and signal, respectively. Positive sign is associated with forward direction, negative one with backward direction. The overlap integral between the normalized optical mode intensity and the population concentrations of the energy levels is given by the following equation:

$$n_i(z, \nu) = \int_{\Omega_{\mathrm{d}}} N_i(x, y, z)|E(x, y, \nu)|^2 \,\mathrm{d}x\mathrm{d}y \tag{4}$$

where Ω_{d} is the rare earth-doped region.

Equations (2) and (3) are integrated with the boundary conditions imposed by the laser mirrors:

$$\begin{cases} P_{\mathrm{s}}^{-}(L) = R_2 P_{\mathrm{s}}^{+}(L) \\ P_{\mathrm{s}}^{+}(0) = R_1 P_{\mathrm{s}}^{-}(0) \end{cases} \tag{5}$$

In the simulation, dopant concentrations lower than $N_{\mathrm{Dy}} = 6 \times 10^{25}\mathrm{ions/m^3}$ are considered in order to avoid the glass devitrification.

By considering the novel pumping scheme in which two pumps, #1 and #2, at the wavelengths $\lambda_{\mathrm{p1}} = 2850\,\mathrm{nm}$ and $\lambda_{\mathrm{p2}} = 4092\,\mathrm{nm}$, respectively, are injected in the laser cavity, a high efficiency is reached. The two pumps populate the $^6\mathrm{H}_{13/2}$ and $^6\mathrm{H}_{11/2}$ dysprosium energy levels. As result, the laser emission at the wavelength $\lambda_{\mathrm{s}} = 4384\,\mathrm{nm}$ is simulated by integrating Eqs. (2) and (3) with the boundary conditions (5).

Fig. 4 illustrates the optical signal power P_{s} of the Dy^{3+}-doped fiber laser versus the optical cavity length L and dopant concentration N_{Dy}. The input pump #1 power is $P_{\mathrm{p1}}(0) = 50\,\mathrm{mW}$ at the wavelength $\lambda_{\mathrm{p1}} = 2850\,\mathrm{nm}$ and the input pump #2 power is $P_{\mathrm{p2}}(0) = 1000\,\mathrm{mW}$ at the wavelength $\lambda_{\mathrm{p2}} = 4092\,\mathrm{nm}$, the first mirror reflectivity is $R_1 = 99\,\%$, while the second mirror reflectivity is $R_2 = 30\,\%$. The reflectivities of the mirrors at both λ_{p1} and λ_{p2} wavelengths are $R_1 = R_2 = 0\,\%$. A laser signal close to $P_{\mathrm{s}} = 360\,\mathrm{mW}$ can be obtained for the optical cavity length $L = 0.4\,\mathrm{m}$ and dopant concentration $N_{\mathrm{Dy}} = 5 \times 10^{25}\mathrm{ions/m^3}$. This result

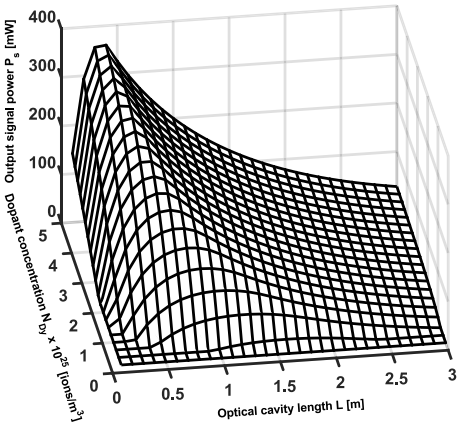

Fig. 4. Optical signal power P_{s} of the Dy^{3+}-doped PCF laser versus optical cavity length L and dopant concentration N_{Dy}. Input pump #1 power $P_{\mathrm{p1}}(0) = 50\,\mathrm{mW}$ at the wavelength $\lambda_{\mathrm{p1}} = 2850\,\mathrm{nm}$; input pump #2 power $P_{\mathrm{p2}}(0) = 1000\,\mathrm{mW}$ at the wavelength $\lambda_{\mathrm{p2}} = 4092\,\mathrm{nm}$; first mirror reflectivity $R_1 = 99\,\%$; second mirror reflectivity $R_2 = 30\,\%$.

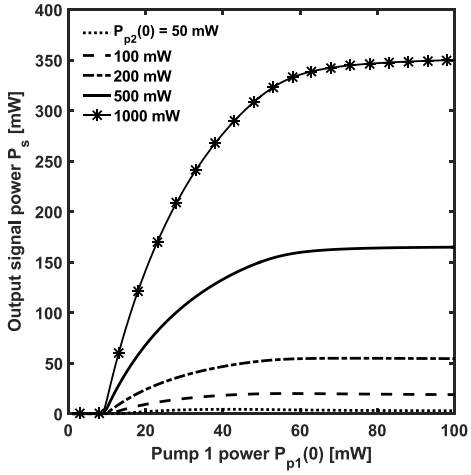

Fig. 5. Optical signal power P_{s} of the Dy^{3+}-doped PCF laser, versus the input pump #1 power $P_{\mathrm{p1}}(0)$ at the wavelength $\lambda_{\mathrm{p1}} = 2850\,\mathrm{nm}$ for different input pump #2 powers at the wavelength $\lambda_{\mathrm{p2}} = 4092\,\mathrm{nm}$, $P_{\mathrm{p2}}(0) = 50\,\mathrm{mW}$ (dotted curve), $P_{\mathrm{p2}}(0) = 100\,\mathrm{mW}$ (dashed curve), $P_{\mathrm{p2}}(0) = 200\,\mathrm{mW}$ (dash-dot curve), $P_{\mathrm{p2}}(0) = 500\,\mathrm{mW}$ (solid curve), $P_{\mathrm{p2}}(0) = 1000\,\mathrm{mW}$ (solid curve with asterisk markers). Optical cavity length $L = 0.5\,\mathrm{m}$; dopant concentration $N_{\mathrm{Dy}} = 4 \times 10^{25}\mathrm{ions/m^3}$; first mirror reflectivity $R_1 = 99\,\%$; second mirror reflectivity $R_2 = 30\,\%$.

is particularly interesting since poor laser slope efficiencies (close to 10%–15%) are reported in literature for different pumping schemes [3]. The above-mentioned literature results are in good agreement with those found by our code when the same cases are investigated.

Fig. 5 illustrates the optical signal power P_{s} of the Dy^{3+}-doped PCF laser, versus the input pump #1 power $P_{\mathrm{p1}}(0)$ for different input pump #2 powers, $P_{\mathrm{p2}}(0) = 50\,\mathrm{mW}$ (dotted curve), $P_{\mathrm{p2}}(0) = 100\,\mathrm{mW}$ (dashed curve), $P_{\mathrm{p2}}(0) = 200\,\mathrm{mW}$ (dash-dot curve), $P_{\mathrm{p2}}(0) = 500\,\mathrm{mW}$ (solid curve), $P_{\mathrm{p2}}(0) = 1000\,\mathrm{mW}$ (solid curve with asterisk markers). The optical cavity length is $L = 0.5\,\mathrm{m}$, the dopant concentration is

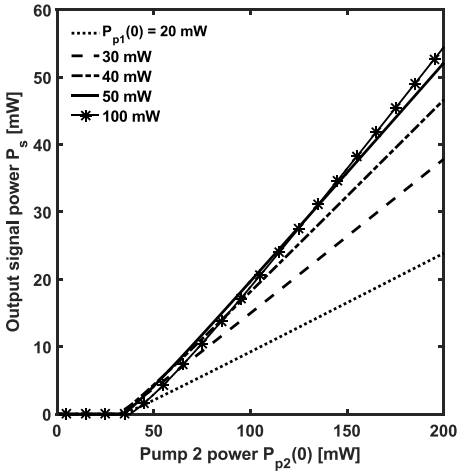

Fig. 6. Optical signal power P_s of the Dy^{3+}-doped PCF laser, versus the input pump #2 power $P_{p2}(0)$ at the wavelength $\lambda_{p2} = 4092$ nm, for different input pump #1 powers at the wavelength $\lambda_{p1} = 2850$ nm, $P_{p1}(0) = 20$ mW (dotted curve), $P_{p1}(0) = 30$ mW (dashed curve), $P_{p1}(0) = 40$ mW (dash-dot curve), $P_{p1}(0) = 50$ mW (solid curve), $P_{p1}(0) = 100$ mW (solid curve with asterisk markers). Optical cavity length $L = 0.5$ m; dopant concentration $N_{Dy} = 4 \times 10^{25}$ ions/m^3; first mirror reflectivity $R_1 = 99\,\%$; second mirror reflectivity $R_2 = 30\,\%$.

$N_{Dy} = 4 \times 10^{25}$ions/m^3, the first mirror reflectivity is $R_1 = 99\,\%$ and the second mirror reflectivity is $R_2 = 30\,\%$. All the curves exhibit a slope which strongly decreases for input pump #1 power $P_{p1}(0)$ higher than 50 mW-60 mW. For the input pump #1 power $P_{p1}(0) = 100$ mW, all the simulated signal powers are close to their saturation values (maximum values obtained by increasing $P_{p1}(0)$).

Fig. 6 depicts the signal power P_s of the Dy^{3+}-doped PCF laser, versus the input pump #2 power $P_{p2}(0)$, for different input pump #1 powers, $P_{p1}(0) = 20$ mW (dotted curve), $P_{p1}(0) = 30$ mW (dashed curve), $P_{p1}(0) = 40$ mW (dash-dot curve), $P_{p1}(0) = 50$ mW (solid curve), $P_{p1}(0) = 100$ mW (solid curve with asterisk markers). The other laser parameters are the same of Fig. 5. The laser characteristics are linear with respect to $P_{p2}(0)$. The slope efficiency increases by increasing the input pump #1 $P_{p1}(0)$ power. For input pump #1 power larger than $P_{p1}(0) = 50$ mW the slope efficiency slightly increases. A slope efficiency close to 36 % and a laser signal power close to $P_s = 54$ mW is obtained by employing the input pump powers $P_{p1}(0) = 100$ mW and $P_{p2}(0) = 200$ mW (solid curve with asterisk markers). The slope efficiency can be increased till about 38 % by considering an optimized cavity length close to $L = 40$ cm, as it can be inferred from Fig. 4. The slope efficiency is calculated by considering only the pump 2 power $P_{p2}(0)$. However, it is almost coincident with the efficiency calculated by considering both P_{p1} and P_{p2} powers if $P_{p1}(0)$ is much lower than $P_{p2}(0)$ as in Fig. 4.

The simulations promise a feasible high beam quality laser in the Mid-IR range. Possible drawbacks could be related to the construction of the multimode combiner which requires a good control of chalcogenide fiber fusion. Other crucial points are related to the optimization of the effective PCF losses and of the grating writing on chalcogenide fiber core.

III. Conclusion

A novel pumping configuration optimized for a Mid-IR Dy^{3+}-doped PCF laser is proposed for the first time. An efficient and high beam quality laser source at the wavelength $\lambda_s = 4384$ nm is simulated. A slope efficiency of about 33 % is calculated for the input pump #1 power $P_{p1} = 50$ mW at the wavelength $\lambda_{p1} = 2850$ nm and the input pump #2 power $P_{p2} = 1000$ mW at the wavelength $\lambda_{p2} = 4092$ nm, with first mirror reflectivity $R_1 = 99\,\%$ and second mirror reflectivity $R_2 = 30\,\%$. The employment of commercial QCL pump lasers at slightly shorter wavelengths makes the system feasible and encourages the authors to construct the prototype. Since possible drawbacks could be related to the construction of the multimode chalcogenide combiner, alternative coupling techniques, based e.g. on lenses and objective, could be employed for the laser set-up implementation. Novel PCF-based fiber lasers will enlarge the offer of Mid-IR light sources, paving the way to good beam quality, narrow linewidth single-frequency operation and ultra-short pulse generation.

References

[1] A. B. Seddon, Z. Tang, D. Furniss, S. Sujecki, and T. M. Benson, "Progress in rare-earth-doped mid-infrared fiber lasers," *Opt. Exp.*, vol. 18, no. 25, p. 26704–26719, Dec. 2010.

[2] L. Sojka *et al.*, "Study of mid-infrared laser action in chalcogenide rare earth doped glass with Dy^{3+}, Pr^{3+} and Tb^{3+}," *Opt. Mater. Exp.*, vol. 2, no. 11, pp. 1632–1640, Nov. 2012.

[3] S. Sujecki *et al.*, "Modelling of a simple Dy^{3+} doped chalcogenide glass fibre laser for mid-infrared light generation," *Opt. Quantum Electron.*, vol. 42, no. 2, pp. 69–79, 2010.

[4] R. S. Quimby, L. B. Shaw, J. S. Sanghera, and I. D. Aggarwal, "Modeling of cascade lasing in Dy: Chalcogenide glass fiber laser with efficient output at 4.5 μm," *IEEE Photon. Technol. Lett.*, vol. 20, no. 2, pp. 123–125, Jan. 15, 2008.

[5] A. D. Orazio, M. De Sario, C. Giasi, L. Mescia, V. Petruzzelli, and F. Prudenzano, "Design of planar optic sensors for hydrocarbon detection," *Opt. Quantum Electron.*, vol. 36, no. 6, pp. 507–526, 2004.

[6] D. D. Hudson, "Short pulse generation in mid-IR fiber lasers," *Opt. Fiber Technol.*, vol. 20, no. 6, pp. 631–641, Dec. 2014.

[7] F. Starecki *et al.*, "Mid-IR optical sensor for CO2 detection based on fluorescence absorbance of Dy3+:Ga5Ge20Sb10S65 fibers," *Sens. Actuator B, Chem.*, vol. 207, no. 5, pp. 518–525, Sep. 2015.

[8] M. Ebrahim-Zadeh, S. Chaitanya Kumar, and K. Devi, "Yb-fiber-laser-pumped continuous-wave frequency conversion sources from the mid-infrared to the ultraviolet," *IEEE J. Sel. Topics Quantum Electron.*, vol. 20, no. 5, pp. 350–372, Sep. 2014.

[9] F. Prudenzano *et al.*, "Design of Er^{3+}-doped chalcogenide glass laser for MID-IR application," *J. Non-Cryst. Solids*, vol. 355, nos. 18–21, pp. 1145–1148, 2009.

[10] L. Mescia, P. Bia, M. De Sario, A. Di Tommaso, and F. Prudenzano, "Design of mid-infrared amplifiers based on fiber taper coupling to erbium-doped microspherical resonator," *Opt. Exp.*, vol. 20, no. 7, pp. 7616–7629, Mar. 2012.

[11] M. De Sario *et al.*, "Feasibility of Er^{3+}-doped, Ga5Ge20Sb10S65 chalcogenide microstructured optical fiber amplifiers," *Opt. Laser Technol.*, vol. 41, no. 1, pp. 99–106, 2009.

[12] F. Prudenzano, L. Mescia, L. Allegretti, V. Moizan, V. Nazabal, and F. Smektala, "Theoretical study of cascade laser in erbium-doped chalcogenide glass fibers," *Opt. Mater.*, vol. 33, no. 2, pp. 241–245, 2010.

[13] L. Mescia, P. Bia, O. Losito, and F. Prudenzano, "Design of mid-IR Er^{3+}-doped microsphere laser," *IEEE Photon. J.*, vol. 5, no. 4, pp. 631–641, Aug. 2013.

[14] L. Mescia *et al.*, "Optimization of the design of high power Er^{3+}/Yb^{3+}-codoped fiber amplifiers for space missions by means of particle swarm approach," *IEEE J. Sel. Topics Quantum Electron.*, vol. 20, no. 5, pp. 484–491, Sep./Oct. 2014.